

RELATIVE HUMIDITY-INDUCED REVERSIBLE HYDRATION OF SULFATE-INTERCALATED LAYERED DOUBLE HYDROXIDES

S. RADHA¹, K. JAYANTHI¹, JOSEF BREU^{2,*}, AND P. VISHNU KAMATH^{1,*}

¹ Department of Chemistry, Central College, Bangalore University, Bangalore-5600 01, India

² Department of Inorganic Chemistry I, University of Bayreuth, Bayreuth, Germany

Abstract—Layered double hydroxides (LDH) are extremely important materials for industrial processes and in the environment, and their physical-chemical behavior depends in large part on their hydration state, but the characterization of these hydration effects on their properties are incomplete. The present study was designed to explore the interpolytype transitions induced by variation in the ambient humidity among LDHs. The cooperative behavior of intercalated water molecules resulted in a sudden, single-step, reversible dehydration of the [Zn-Cr-SO₄] LDH. The [Zn-Al-SO₄] LDH provided an interesting contrast with (1) the coexistence of the end members of the hydration cycle over the 40–20% relative humidity range during the dehydration cycle, and (2) a random interstratified intermediate in the hydration cycle. These observations showed that the [Zn-Al-SO₄] LDH offered sites having a range of hydration enthalpies, whereby, at critical levels of hydration (20–40%), the non-uniform swelling of the structure resulted in an interstratified phase. The variation in domain size during reversible hydration was also responsible for the differences observed in the hydration vs. the dehydration pathways. This behavior was attributed to the distortion in the array of hydroxyl ions which departs from hexagonal symmetry on account of cation ordering as shown by structure refinement by the Rietveld method. This distortion was much less in the [Zn-Cr-SO₄] LDH, whereby the nearly hexagonal array of hydroxyl ions offered sites of uniform hydration enthalpy for the intercalated water molecules. In this case, all the water molecules experienced the same force of attraction and dehydrated reversibly in a single step. The changes in basal spacing were also accompanied by interpolytype transitions, involving the rigid translations of the metal hydroxide layers relative to one another.

Key Words—Cation Ordering, Layered Double Hydroxides, Polytype Transformation.

INTRODUCTION

Layered double hydroxides (LDHs) are a class of inorganic solids also called anionic clays. The better-known cationic clays consist of negatively charged aluminosilicate layers and intercalated cations (Weiss, 1963). The LDHs consist of positively charged metal hydroxide layers with anions included in the interlayer region. The metal hydroxide layers are derived from the structure of the mineral brucite (Oswald and Asper, 1977) and have the composition $[M_{(1-x)}^{II}M_x^{III}(\text{OH})_2](A^{n-})_{x/n}\cdot y\text{H}_2\text{O}$ ($M^{II} = \text{Mg, Fe, Ni, Co, Cu, Zn}$; $M^{III} = \text{Al, Cr, Fe}$; $A = \text{Anion}$; $0.2 \leq x \leq 0.33$) (Reichle, 1986). The present study dealt with LDHs having the layer $[\text{Zn}_{0.67}\text{M}_{0.33}(\text{OH})_2]^{0.33+}$ ($M = \text{Cr, Al}$) (Boehm *et al.*, 1977). Anions and water molecules were incorporated into the interlayer region to restore charge neutrality. Two questions are often asked: (1) Is the position of the M' ion ordered with respect to the divalent cation or is the metal hydroxide layer cation disordered (Serna *et al.*, 1982)? (2) In what manner are the atoms packed within the interlayer?

Evidence in favor of cation ordering is provided by an array of techniques such as extended X-ray absorption fine structure (Vucelic *et al.*, 1997; Bigey *et al.*, 1997; Roussel *et al.*, 2000, 2001), magic angle spinning-nuclear magnetic resonance (Sideris *et al.*, 2008, 2012; Cadars *et al.*, 2011), and X-ray diffraction (XRD) (Krivovichev *et al.*, 2010; Radha and Kamath, 2013). Cation ordering generates a large unit cell with $a = \sqrt{n \times a_0}$ ($n = 3$ for $x = 0.33$) (Hofmeister and Platen, 1992).

The second question is more difficult to answer given the inherent disorder in the interlayer, the high symmetry of the host layer, and the low atomic scattering factors of anions comprising light atoms. Where structure models are offered, the anions are located in the sites of high degeneracy with low site-occupancy factors (Besserguenev *et al.*, 1997). Simulations based on molecular dynamics generally predict that the anion occupies a site close to that of the trivalent cations, which is the seat of the positive charge on the metal hydroxide layer (Li *et al.*, 2006). The locations of the intercalated water molecules are also not determined with certainty. The O atoms of the intercalated water are often shown to share the same crystallographic sites as those of anions in the interlayer (Evans and Slade, 2005). Further LDHs intercalated with sulfate ions exhibit basal spacings ranging from 7.8 to 11.2 Å, based on the

* E-mail address of corresponding authors:
josef.breu@uni-bayreuth.de, vishnukamath8@hotmail.com
DOI: 10.1346/CCMN.2014.0620105

amount of intercalated water (Drits and Bookin, 2001). Likewise, LDHs intercalated with organic anions such as carboxylates exhibit humidity-driven hydration-dehydration phenomena, owing to their large hydration enthalpies, a fact that has been exploited for the facile aqueous exfoliation of these materials (Hibino and Kobayashi, 2005). The hydration-dehydration behavior of many simple inorganic anions in the [Mg-Al] system with different compositions of the metal hydroxide layer were investigated thoroughly by Iye *et al.* (2007) who found that, among others, the [Mg-Al] LDHs intercalated with SO_4^{2-} , ClO_4^- , and I^- exhibited basal spacing variation on being exposed to different relative humidities. While I^- and ClO_4^- -intercalated LDHs exhibited an ordered interstratified intermediate phase during hydration, SO_4^{2-} -LDH showed a one-step change in the basal spacing. Similar studies of [Mg-Al] and [Li-Al] LDHs intercalated with different anions were reported by Hou and Kirkpatrick (2000, 2002) and Hou *et al.* (2003). Based on those observations with different anions, the hydration behavior among LDHs were classified into three types: significantly expandable, slightly expandable, and non-expandable.

The diverse behavior of intercalated water molecules in different LDHs is on account of the different bonding interactions operating on them in the interlayer. These include (1) the hydration enthalpy of the anions, (2) the strength of the H-bonding with the metal hydroxide layer, and (3) the hydrogen bonding between the intercalated water molecules.

Among these, the last factor can vary considerably with the degree of hydration, leading to cooperative effects at the extreme end.

Dehydration results in a decrease in the number density of atoms in the interlayer. The objective of the present study was to examine if dehydration of the interlayer leads to a change in the stacking sequence of the metal hydroxide layer, thereby bringing about interpolytype transitions. Another objective was to examine if the differences in the structures of the two LDHs [Zn-M-SO₄] ($M = \text{Cr}, \text{Al}$) affect their respective hydration behaviors.

EXPERIMENTAL

Preparation of LDHs

Reagents used without further purification were ZnCl_2 (95% ZnCl_2 and $\leq 5\%$ zinc oxide chloride), Al_2SO_4 (98%), and ZnSO_4 (99.5%) from Merck, India, and CrCl_3 (99%) and Na_2SO_4 (99%) from Aldrich Chemical Co., USA. [Zn-Al-SO₄] and [Zn-Cr-SO₄] LDHs were prepared by coprecipitation at constant pH values of 10 and 5, respectively. In a typical preparation, 50 mL of the mixed-metal salt solution (sulfates in the case of the [Zn-Al] LDH and chlorides in the case of the [Zn-Cr] LDH; $[\text{Zn}^{2+}]/[\text{M}^{3+}] = 2$; $M = \text{Al}, \text{Cr}$, total metal concentration 0.4 M) was added at a dosing rate of

0.14 mL/min to a reaction vessel (volume 400 mL) containing Na_2SO_4 salt solution (100 mL) in 10-times excess of the stoichiometric requirement. A constant pH was maintained during the synthesis by simultaneous addition of 0.5 N NaOH using a Metrohm Model 718 STAT Titrino (Herisau, Switzerland) operating in the pH STAT mode. The temperature was kept constant at 60°C and N_2 was bubbled continuously. Boiled, deionized, Millipore Academic Water Purification System (Molsheim, France)-water was used throughout the synthesis to avoid possible carbonate contamination. The resulting slurry was aged for 15 h and separated by centrifugation followed by repeated washing with decarbonated water and finally with acetone. The precipitate obtained was then dried at 60°C and stored in a desiccator.

Characterization

Both the samples were characterized by X-ray powder diffraction (XRPD) using a Bruker D8 Advance powder diffractometer (Karlsruhe, Germany) (source $\text{CuK}\alpha$ radiation, $\lambda = 1.5418 \text{ \AA}$). Data were collected at a continuous scan rate of $1^\circ 2\theta \text{ min}^{-1}$. For structure refinement by the Rietveld method, data were collected over a 2θ range of $5-70^\circ$ (step size $0.02^\circ 2\theta$, counting time 10 s/step). *In situ* measurements of XRPD patterns at different relative humidities were carried out using a PANalytical X'pert X-ray diffractometer (Almelo, The Netherlands) ($\text{CuK}\alpha$ radiation, $\lambda = 1.5418 \text{ \AA}$, Bragg-Brentano geometry) equipped with an X'celerator Scientific RTMS detector and an Anton Paar temperature humidity chamber (Graz, Austria) driven by a VTI Corp. RH-200 humidity generator (Graz, Austria). Measurements were done at different relative humidity (RH) values ranging from $<5\%$ (referred to hereafter as 0%) to 98% (referred to hereafter as 100%) at intervals of 10%. The sample was allowed to equilibrate for a period of 60 min at each RH value before performing the XRD measurements. Data were collected from 5 to $70^\circ 2\theta$ with a step size of $0.017^\circ 2\theta$ at a scan rate of $1^\circ/\text{min}$.

Infrared spectra of the samples were recorded using a Bruker Alpha-P FTIR spectrometer (Ettlingen, Germany) (ATR mode, diamond crystal, $400-4000 \text{ cm}^{-1}$, 4 cm^{-1} resolution). Thermogravimetric analyses were carried out using a Mettler Toledo 851° TGA/SDTA system (Schwerzenbach, Switzerland). The samples were dried at 100°C for 30 min in the TG balance and then the temperature was ramped from 100 to 800°C at a heating rate of $5^\circ\text{C}/\text{min}$ under N_2 flow. The Zn and Al contents in the LDH were estimated by means of atomic absorption spectroscopy using a Varian Model AA240 atomic absorption spectrometer (Victoria, Australia). The sulfate content present was estimated by wet chemical analysis by precipitation as BaSO_4 . The $[\text{Zn}]/[\text{M}]$ ratio ($M = \text{Al}, \text{Cr}$) was close to 2 in all the samples, which is consistent with earlier reports (Boclair *et al.*, 1999). In all cases, the estimated sulfate content

was lower than the stoichiometric requirement to balance the positive charge. This deficiency was made up by the inclusion of carbonate ions to arrive at an approximate formula for each of the LDHs. In each case, the carbonate content was negligible (~ 0.02 mol per empirical formula unit) and, for all practical purposes, the LDHs were treated as though they were carbonate-free and abbreviated with the symbol $[\text{Zn-}M\text{-SO}_4]$ ($M = \text{Cr, Al}$).

Computational studies

The powder patterns obtained were indexed using the program *PROZSKI* (Lasocha and Lewiniski, 1994) and the figure of merit (FM) obtained. *DIFFaX* (Treacy *et al.*, 1991, 2000), a FORTRAN-based computer program, was used to simulate the XRPD patterns corresponding to different polytypes and model structural disorder where necessary. The *DIFFaX* formalism treats a solid as a stacking of layers of atoms. The position coordinates corresponding to atoms present in the metal hydroxide layer and the interlayer were defined according to the published structure models [CC no: 91860 (1*H* polytype); 91859 (3*R*₁ polytype)]. Different polytypes were simulated by varying the stacking vectors.

The XRPD patterns of different polytypes differed from each other in the positions and relative intensities of the reflections appearing in the mid-2 θ region (30–55°2 θ). Polytypes were identified primarily by comparing the observed peak positions with those expected of different polytypes. The reflections were also indexed to obtain the refined cell parameters, an exercise which yielded the crystal symmetry. The refined c parameter yielded the number of layers per unit cell. A full profile match of the observed pattern with that of the corresponding polytype was then attempted by *DIFFaX* simulations. Where the samples were ordered, a full profile match between the observed and calculated XRPD patterns was obtained. In some instances, there was a mismatch in the relative intensities of selected reflections. Such mismatch, if any, arose due to: (1) orientational effects of lamellar crystallites which accentuate the intensities of the basal reflections, and (2) structural disorder due to the incorporation of small proportions of stacking faults

which affect reflections appearing in the mid-2 θ region. In this work, minor variations in the relative intensities of reflections appearing in mid-2 θ region were ignored for the purpose of polytype identification.

The structure of the $[\text{Zn-Al-SO}_4]$ LDH was refined by the Rietveld method using the *GSAS* software package (Larson and Von Dreele, 2004). A TCH pseudo-Voigt line-shape function (Profile function 2) with seven variables was used to fit the experimental profile. The refinable profile parameters included asymmetric peak shape, sample displacement, and parameters U_G , V_G , and W_G and X_L and Y_L for Gaussian and Lorentzian contributions, respectively.

During refinement, restraints were placed on the S–O (1.4 ± 0.1 Å) bond length and O–S–O bond angle ($109 \pm 1^\circ$) in the initial cycles of the refinement. The position coordinates and SOF (Site occupancy factors) were refined one atom at a time, keeping the parameters of other atoms fixed in order to achieve a stable refinement. In the final cycles of the refinement, the restraints placed on the sulfate structure were removed while keeping the structure of the metal hydroxide layer fixed. Attempts to refine the structure by freeing up all the parameters at the same time did not lead to stable refinement.

RESULTS

$[\text{Zn-Cr-SO}_4]$ LDH

The as-prepared $[\text{Zn-Cr-SO}_4]$ LDH exhibited a basal reflection at $9.8^\circ 2\theta$. The observed reflections were indexed to a cell of hexagonal symmetry with a refined $c = 8.93$ Å (Table 1, Supporting Information SI 1, available from the journal's data depository at <http://www.clays.org/JOURNAL/JournalDeposits.html>) which shows that the compound belongs to the 1*H* polytype (see trace labeled 'Ambient' in Figure 1). Composition analysis yielded the approximate formula $[\text{Zn}_{0.67}\text{Cr}_{0.33}(\text{OH})_2][(\text{SO}_4)_{0.148}(\text{CO}_3)_{0.018}] \cdot 0.4 \text{H}_2\text{O}$.

The observed basal spacing corresponds to a hydrated structure with a layer of intercalated water molecules. Therefore, the sample was first dehydrated by equilibration at RH $\leq 5\%$ (3 h). The first basal spacing shifted to 8.6 Å ($10.1^\circ 2\theta$). The reflections in the mid-2 θ region

Table 1. Composition, relative humidity, corresponding cell parameters, figure of merit (FM), and polytype of the $[\text{Zn-}M\text{-SO}_4]$ ($M = \text{Cr, Al}$) LDHs.

Composition (Relative Humidity)	a (Å)	c (Å)	FM	Polytype
$[\text{Zn}_{0.67}\text{Cr}_{0.33}(\text{OH})_2][(\text{SO}_4)_{0.148}(\text{CO}_3)_{0.018}] \cdot 0.4\text{H}_2\text{O}$ (Ambient)	3.11	8.93	61.2	1 <i>H</i>
0% RH	3.11	25.65	24.3	3 <i>R</i> ₁
10% RH	3.13	8.95	55.2	1 <i>H</i>
100% RH	3.12	32.7	23.0	3 <i>R</i> ₁
$[\text{Zn}_{0.67}\text{Al}_{0.33}(\text{OH})_2][(\text{SO}_4)_{0.144}(\text{CO}_3)_{0.02}] \cdot 1.03\text{H}_2\text{O}$ (Ambient)	5.34	11.14	23.39	1 <i>H</i>
10% RH	3.06	25.77	18.6	3 <i>R</i> ₁

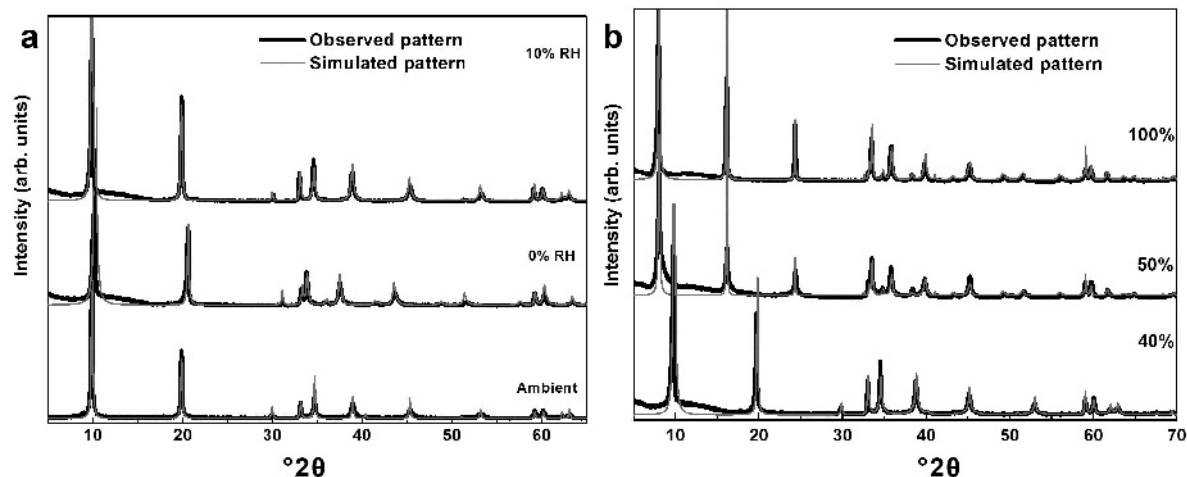


Figure 1. XRPD pattern of the as-prepared $[\text{Zn-Cr-SO}_4]$ LDH and under various relative humidities from 0 to 100% obtained during the hydration cycle. In each case the observed pattern is overlain with the corresponding *DIFFaX* simulation.

shifted to new positions and were then indexed to a cell of rhombohedral symmetry ($-h + k + l = 3n$, Supporting Information SI. 1). The observation of the 012, 015, and 108 reflections, to the exclusion of the 104 and 107 reflections, was indicative of the $3R_1$ polytype. The refined cell parameters ($a = 3.11 \text{ \AA}$, $c = 25.65 \text{ \AA}$; FM = 24.3) corresponded to a unit cell of three layers and this sample was, thus, referred to as an $8.6 \text{ \AA-}3R_1$ polytype. On increasing the RH to 10% (Figure 1), the $8.6 \text{ \AA-}3R_1$ phase reverted to the as-prepared $8.8 \text{ \AA-}1H$ phase, which remained stable with a slight increase in basal spacing to 9.0 \AA until the RH reached a value of 40%. At 50% RH a sudden one-step increase in the basal spacing to 11 \AA was accompanied by the structural transformation to a new $3R_1$ phase. The $3R_1$ polytype thus formed remained stable up to >98% RH (Table 1, Supporting Information SI. 1).

During dehydration, the $11 \text{ \AA-}3R_1$ hydrated phase remained stable until 40% RH. At 30% RH, a sudden one-step decrease in basal spacing to 8.8 \AA with the polytype transformation from $3R_1$ to $1H$ was observed (Figure 2). Further decrease in RH stepwise to <5% generated the $8.6 \text{ \AA-}3R_1$ phase as earlier. The transformations observed during the hydration cycle were, thus, reversible. The basal spacing variations occurring during the hydration process are shown in Supporting Information SI. 2 and the humidity-driven interpolytype transformations are summarized in Supporting Information SI. 3.

Some of the results described here are similar to the reports by Khaldi *et al.* (1997) which were *ex situ* measurements. Structural changes at different water-vapor pressures were reported by Mostarih and de Roy (2006) and compared to those under vacuum.

$[\text{Zn-Al-SO}_4]$ LDH

The XRPD pattern of the as-prepared $[\text{Zn-Al-SO}_4]$ LDH exhibited a basal spacing of 10.9 \AA ($8.1^\circ 2\theta$)

(Figure 3a) corresponding to a bilayer arrangement of water molecules in the interlayer. The XRPD pattern is similar to that expected of a $1H$ polytype ($a = 5.34 \text{ \AA}$, $c = 11.09 \text{ \AA}$, FM = 23.4, Table 1, Supporting Information SI.4). The approximate formula derived on the basis of composition analysis was $[\text{Zn}_{0.67}\text{Al}_{0.33}(\text{OH})_2][(\text{SO}_4)_{0.144}(\text{CO}_3)_{0.02}] \cdot 1.03 \text{ H}_2\text{O}$.

The larger a parameter of this phase ($a = 5.34 \text{ \AA} = \sqrt{3} \times a_o$), compared to that of the more prevalent phases ($a_o = 3.11 \text{ \AA}$), corresponded to a cation-ordered cell and the corresponding supercell reflections 100 and 101 were observed at 19.2 and $20.8^\circ 2\theta$, respectively. The structure of this phase was refined using the cation-ordered structure model (space group $P\bar{3}$) proposed for the $[\text{Zn-Cr-SO}_4]$ LDH (Radha and Kamath, 2013). Details of the structure (Supporting Information SI. 5–9) are available from the Cambridge Crystallography Data Centre (CCDC 975959).

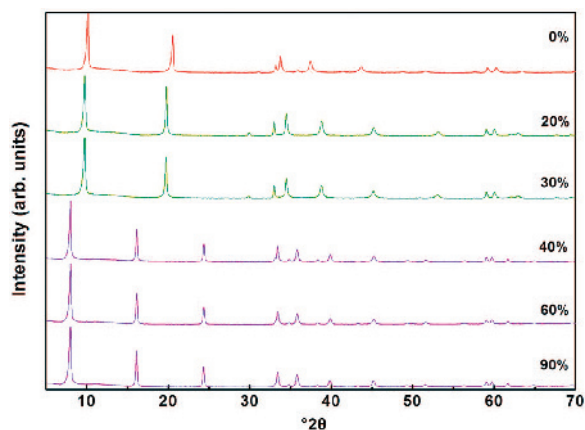


Figure 2. Evolution of XRPD patterns of $[\text{Zn-Cr-SO}_4]$ LDH during the dehydration cycle as a function of varying relative humidity.

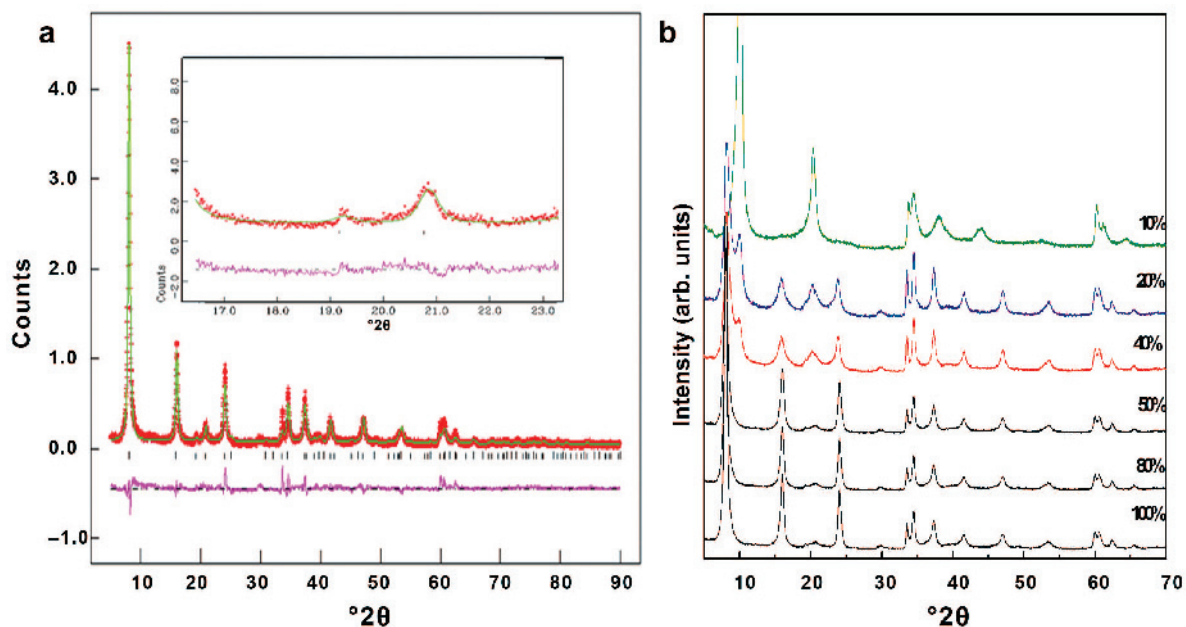


Figure 3. (a) Rietveld fit of the XRPD pattern of the $[\text{Zn-Al-SO}_4]$ LDH. (Inset) Details of the fit of the supercell reflections. (b) Evolution of XRPD patterns of $[\text{Zn-Al-SO}_4]$ LDH during the dehydration cycle as a function of relative humidity.

The as-prepared phase in the $[\text{Zn-Al}]$ system is highly hydrated and on equilibration at RH $\sim 98\%$ for 3 h, no further hydration was observed. On step-wise reduction of the relative humidity, the 10.9 \AA - $1H$ phase was stable up to a RH value of 50%. At 40% RH, an 8.8 \AA ($10.1^\circ 2\theta$) reflection emerged along with the 10.9 \AA peak, indicating the coexistence of two different phases (Figure 3b). The 8.8 \AA peak and its higher order at $\sim 4.4 \text{ \AA}$ ($20.4^\circ 2\theta$) grew in intensity with further decrease in RH and continued to coexist with the 10.9 \AA - $1H$ phase up to 20% RH. The simultaneous appearance of the basal reflections of the end members showed that the sample

at the 40–20% RH range is a physical mixture of hydrated phase and the dehydrated phase. At 10% RH the biphasic mixture was completely transformed into the 8.8 \AA - $3R_1$ phase (Table 1, Supporting Information SI. 4). This $3R_1$ phase remained stable below 5% RH with a slight decrease in basal spacing to 8.7 \AA .

The dehydrated phase was then subjected to the hydration cycle, with a stepwise increase in RH from 10% to 100% (Figure 4). The 8.7 \AA - $3R_1$ phase was observed until 10% RH. On increasing the RH to 20%, the basal reflection was split into two, indicating the coexistence of two phases corresponding to 8.8 \AA and

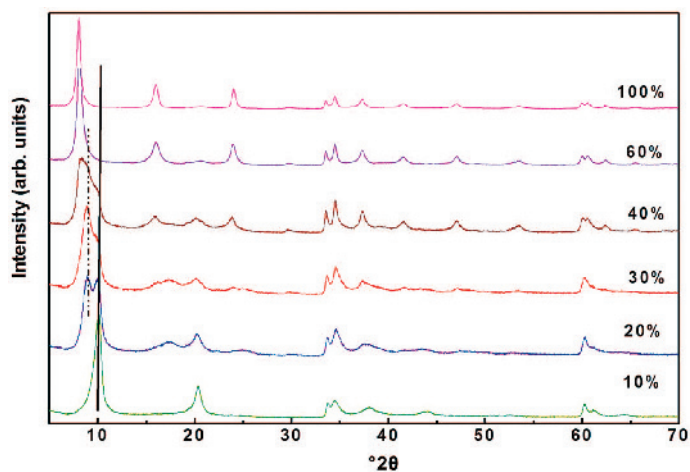


Figure 4. Evolution of the XRPD patterns of $[\text{Zn-Al-SO}_4]$ LDH during the hydration cycle as a function of relative humidity. The solid vertical line corresponds to the basal spacing of the dehydrated phase. The broken vertical line corresponds to the peak due to the staged phase.

9.9 Å. The 9.9 Å phase observed here corresponded to a random interstratified phase of the two end members ($c = 11$ Å and 8.8 Å) with a ~1:1 ratio. At 30% RH the 9.9 Å phase was dominant. Further increase in RH merged the two basal reflections and then gradually shifted it toward higher d values and a series of irrational basal reflections observed at 10.5 Å (40% RH), 10.6 Å (50% RH), 10.7 Å (60% RH), and 10.8 Å (70% RH) corresponding to increasing amounts of the bilayer hydrate being incorporated into the stacking before forming a fully hydrated phase corresponding to 11 Å at ~98% RH (Supporting Information SI. 2 and 10). These are the various randomly interstratified phases corresponding to different proportions of the end members, demonstrating Mering's principle (1946) that is widely used among cationic clays to demonstrate interstratification phenomena. The stacking sequence of the adjacent metal hydroxide layers was different in the two end members of the hydration cycle. Consequently, at intermediate degrees of hydration, stacking modes corresponding to both end members coexisted as was shown by the presence of different hkl reflections of the two end members concomitantly with the irrational $00l$ series (Figure 5). The basal reflections in the observed pattern appeared at positions intermediate between those expected of the end members in keeping with the predictions made by Mering's rules for interstratified phases. These observations are unlike those in the dehydration cycle where only the two end members with basal spacings of 8.8 Å and 11 Å, respectively, coexisted.

To conclude, the [Zn-Cr-SO₄] LDH underwent a one-step reversible hydration while in the case of the [Zn-Al-

SO₄] LDH the behavior during hydration was different from that during dehydration.

DISCUSSION

The two LDHs studied here have the same composition ($[Zn]/[M] = 2$; $M = Al, Cr$). Both the LDHs are cation-ordered. Cation ordering brings down the crystal symmetry to $P\bar{3}$, compared to the $R\bar{3}m$ crystal symmetry of the cation disordered phase. In a cation-disordered phase, the $[M(OH)_6]$ coordination polyhedron is symmetric (coordination symmetry $\bar{3}m, D_{3d}$), with a single $M(Zn, M^{III})-O$ distance, resulting in a perfectly hexagonal array of hydroxyl ions on either side of the cation layer.

In a cation-ordered metal hydroxide layer, the coordination polyhedron $[M^{III}(OH)_6]$ is regular with a single $M^{III}-O$ ($M^{III} = Al, Cr$) bond distance. The coordination polyhedron around $[Zn(OH)_6]$ is greatly distorted with two different Zn-O bond lengths. The three long bonds define one triangular face of the polyhedron and the three short bonds define the opposite face; this pair of faces is perpendicular to the c crystallographic axis and the stacking direction.

As the position of the cations is centric (z is 0.0 for both Zn and M^{III}), the distortion in the coordination polyhedra is manifest in the distortion of the array of the hydroxyl ions. Three non bonded in-plane O1-O1 (O1: Hydroxyl O atom) distances exist, whereas for a perfectly hexagonal array, as in the $3R_1$ polytype (Radha and Kamath, 2013), only one distance exists at 3.12 Å (Figure 6). A comparison of the hydroxyl ion array in the two LDHs shows that the distortion from

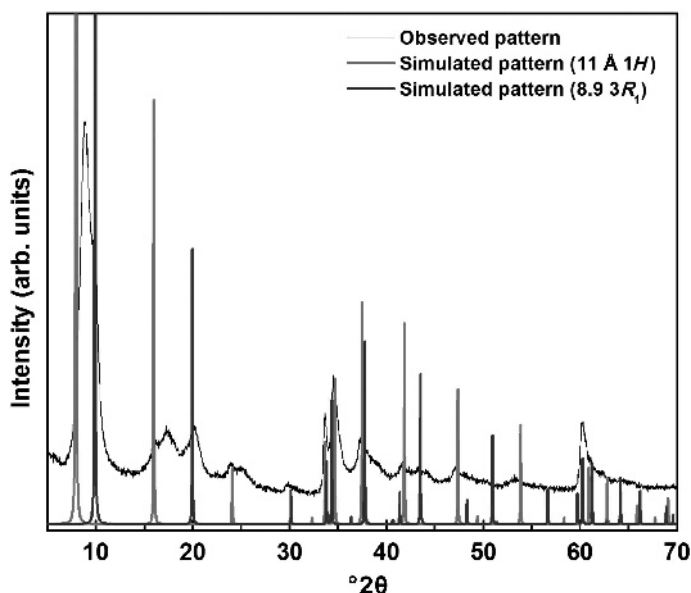


Figure 5. XRPD patterns of [Zn-Al-SO₄] LDH at 30% RH during the hydration cycle overlain with the simulated patterns of the two end members. Peaks unaccounted for by the simulated patterns correspond to the interstratified phase.

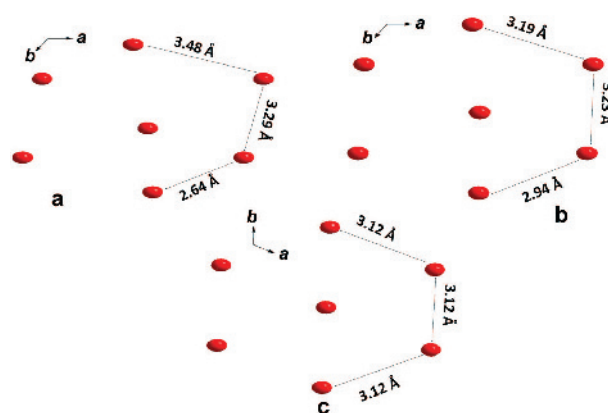


Figure 6. A hydroxyl array of (a) cation-ordered $[\text{Zn-Al-SO}_4]$, (b) cation-ordered $[\text{Zn-Cr-SO}_4]$, and (c) cation-disordered $[\text{Zn-Cr-SO}_4]$.

hexagonal symmetry is much less in $[\text{Zn-Cr-SO}_4]$ (O1–O1: 2.93, 3.19, 3.23 Å) than in $[\text{Zn-Al-SO}_4]$ (O1–O1: 2.64, 3.29, 3.48 Å).

The differences in the hydration-dehydration behavior of these two sulfate-intercalated LDH systems may be interpreted in terms of two competing interactions involving water molecules in the interlayer: (1) hydrogen bonding with the array of hydroxyl ions defining the surface of the metal hydroxide layers; and (2) hydrogen bonding interactions with other intercalated water molecules.

If the array of hydroxyl ions defining the surface of the metal hydroxide layer were to be of perfectly hexagonal symmetry as in a cation disordered structure or only slightly distorted as in $[\text{Zn-Cr-SO}_4]$ LDH, the water molecule would encounter sites of a single hydration enthalpy as offered by a layer having a uniform charge distribution. This would lead to a single-step hydration with sudden and discontinuous swelling followed by single-step dehydration – the cooperative effects introducing hysteresis. Such behavior was observed in $[\text{Zn-Cr-SO}_4]$ LDH and was similar to that observed for most of the synthetic clays (Breu *et al.*, 2001).

In the $[\text{Zn-Al-SO}_4]$ LDH, however, the highly distorted array of hydroxyl ions would offer sites with wide variations in the hydration enthalpy, arising out of a non-uniform charge distribution. The closely spaced hydroxyl ions (O1–O1: 2.64 Å) offer sites of greater hydration enthalpy compared to those more distant from one another (O1–O1: 3.48 Å). In such a situation the forces operating between the array of the hydroxyl ion and the intercalated water also vary with the degree of hydration. The incoming water molecules in the initial stage of the hydration cycle are predominantly influenced by the metal hydroxide layer. As hydration proceeds, the incoming water molecules interact increasingly with other water molecules and are screened from the metal hydroxide layer. Because the interlayer water molecules are disordered, the ingress of water molecules also takes place in a disordered

fashion leading to randomly interstratified phases with irrational basal spacings. Once the LDH is fully hydrated, the $3R_1$ polytype completely transforms to the structure of the $1H$ polytype. The reversible $3R_1 \rightarrow 1H$ transformation is realized by the rigid translations of successive metal hydroxide layers relative to one another.

Another anion closely related to SO_4^{2-} is $\text{S}_2\text{O}_3^{2-}$. The reversible hydration behavior of the $[\text{Zn-Al-S}_2\text{O}_3]$ LDH (Radha *et al.*, 2013) offers an interesting comparison with two significant differences: (1) the end members of the hydration-dehydration cycle both adopt the structure of the $3R_1$ polytype and no detectable interpolytype transitions are noted; and (2) both end members coexist over a significant range of RH values (40–60%). Irrational basal reflections are not observed under any conditions, ruling out the possibility of the existence of interstratified phases. The coexistence of the end members was, therefore, attributed to kinetic factors (Radha *et al.*, 2013).

An explanation based on factors related to kinetics is also plausible for the hydration behavior of the $[\text{Zn-Al-SO}_4]$ LDH. The observation of irrational basal reflections (Figure 5) tilts the balance of judgment in favor of the stabilization of an interstratified phase, however. Why is the hydration cycle different from the dehydration cycle in the $[\text{Zn-Al-SO}_4]$ LDH? Probably because of the domain-size variation which changes with the degree of hydration. A fully hydrated phase would have a larger domain size, due to the uniform and complete ingress of water, into the LDH crystal. As dehydration begins, the water molecules are lost from sites of low hydration enthalpy resulting in XRPD patterns akin to that of a mixed phase. On complete dehydration, the domain size decreases as uneven dehydration causes the breakup of domains. During rehydration, the domains are expected to grow again. Below an average critical domain size, less than the coherent scattering length of the X-rays, however, uneven hydration of the LDH crystallites yields an XRPD pattern akin to that of a randomly interstratified phase.

All these changes are also accompanied by interpolytype transformations between $1H$ and $3R_1$ which are realized by rigid translations of successive metal hydroxide layers relative to one another.

CONCLUSIONS

Structure refinement by the Rietveld fit of the XRPD patterns showed that the metal hydroxide layers are cation ordered in both the [Zn-Cr] and [Zn-Al] LDHs. Cation ordering induces a distortion in the array of hydroxyl ions and consequently in its charge distribution, generating sites of different hydration enthalpies within the interlayer. This distortion was more pronounced in the case of [Zn-Al] than in [Zn-Cr]. The [Zn-Al] LDH underwent non-uniform hydration, therefore, leading to a randomly interstratified intermediate over a range of relative humidity values, whereas the [Zn-Cr] LDH underwent a single-step hydration-dehydration.

ACKNOWLEDGMENTS

The authors from India thank the Department of Science and Technology (DST), and the University Grants Commission (UGC), Government of India (GOI) for financial support. S. R. thanks the German Research Foundation (SFB 840) for supporting a visit to the University of Bayreuth and the Council for Scientific Industrial Research, GOI, for the award of a Senior Research Fellowship. K.J. thanks the UGC, GOI, for a Project Fellowship. P.V.K. is a recipient of the Ramanna Fellowship of the DST, GOI.

Supporting Information: List of Bragg reflections, basal spacing dynamics, reversible dehydration schemes, plot of the crystal structures of [Zn-Al-SO₄] LDH, and the results of the Rietveld refinement.

REFERENCES

- Besserguenev, A.V., Fogg, A.M., Francis, R.J., Price, S.J., and O'Hare, D. (1997) Synthesis and structure of the gibbsite intercalated compounds [LiAl₂(OH)₂]X {X = Cl, Br, NO₃} and [LiAl₂(OH)₆]Cl.H₂O using synchrotron X-ray and neutron powder diffraction. *Chemistry of Materials*, **9**, 241–247.
- Bigey, L., Depege, C., de Roy, A., and Besse, J.P. (1997) EXAFS and XANES study of layered double hydroxides. *Journal de Physique IV*, **7**, 949–950.
- Boclair, J.W., Braterman, P.S., Jiang, J., Lou, S., and Yarberr, F. (1999) Layered double hydroxides stability. 2. Formation of Cr (III)-containing layered double hydroxides directly from solution. *Chemistry of Materials*, **11**, 303–307.
- Boehm, H.P., Steinle, J., and Vieweger, C. (1977) [Zn₂Cr(OH)₆]x.2H₂O, new layer compounds capable of anion exchange and intracrystalline swelling. *Angewandte Chemie*, **16**, 265–266.
- Breu, J., Seidl, W., Stoll, A.J., Lange, K.G., and Probst, T.U. (2001) Charge homogeneity in synthetic fluorohectorite. *Chemistry of Materials*, **13**, 4213–4220.
- Cadars, S., Layrac, G., Gerardin, C., Deschamps, M., Yates, J.R., Tichit, D., and Massiot, D. (2011) Identification and quantification of defects in the cation ordering in Mg/Al layered double hydroxides. *Chemistry of Materials*, **23**, 2821–2831.
- Drits, V.A. and Bookin, A.S. (2001) Crystal structure and X-ray identification of layered double hydroxides. Pp. 39–92 in: *Layered Double Hydroxides: Present and Future* (V. Rives, editor). Nova Science, New York.
- Evans, D.G. and Slade, R.C.T. (2005) *Structural Aspects of Layered Double Hydroxides in Layered Double Hydroxides* (X. Duan and D.G. Evans, editors). Springer, Berlin.
- Hibino, T. and Kobayashi, M. (2005) Delamination of layered double hydroxides in water. *Journal of Materials Chemistry*, **15**, 653–656.
- Hofmeister, W. and Platen, H.V. (1992) Crystal chemistry and atomic order structures in brucite-related double-layer structure. *Crystallography Reviews*, **3**, 3–26.
- Hou, X. and Kirkpatrick, R.J. (2000) Solid-State ⁷⁷Se NMR and XRD study of the structure and dynamic of seleno-anions in hydrotalcite-like compounds. *Chemistry of Materials*, **12**, 1890–1897.
- Hou, X. and Kirkpatrick, R.J. (2002) Interlayer structure and dynamics of ClO₄⁻ layered double hydroxides. *Chemistry of Materials*, **14**, 1195–1200.
- Hou, X., Bish, D.L., Wang, S.L., Johnston, C.T., and Kirkpatrick, R.J. (2003) Hydration, expansion, structure, and dynamics of layered double hydroxides. *American Mineralogist*, **88**, 167–179.
- Iye, N., Fujii, K., Okamoto, K., and Sasaki, T. (2007) Factors influencing the hydration of layered double hydroxides (LDHs) and the appearance of an intermediate second staging phase. *Applied Clay Science*, **35**, 218–227.
- Khalidi, M., de Roy, A., Chaouch, M., and Besse, J.P. (1997) New varieties of zinc-chromium-sulfate lamellar double hydroxides. *Journal of Solid State Chemistry*, **130**, 66–73.
- Krivovichev, S.V., Yakovenchuk, V.N., Zhotova, E.S., Zolotarev, A.A., Pakhomovsky, Y.A., and Ivanyuk, G.Yu. (2010) Crystal chemistry of natural layered double hydroxides. I. Quintinite-2H-2c from Kovdor Alkaline Massif, Kola Peninsula, Russia. *Mineralogical Magazine*, **74**, 821–832.
- Larson, A.C. and Von Dreele, R.B. (2004) General Structure Analysis System (GSAS), Los Alamos National Laboratory Report LAUR 86-748. Los Alamos National Laboratory, Los Alamos, NM.
- Lasocha, W. and Lewiniski, K. (1994) PROSZKI, a system of programs for powder diffraction data analysis Version 2.4. Krakow, Poland.
- Li, H., Ma, J., Evans, D.G., Zhou, T., Li, F., and Duan, X. (2006) Molecular dynamics modeling of the structure and binding energies of α -nickel hydroxides and nickel-aluminum layered double hydroxide containing various interlayer guest anions. *Chemistry of Materials*, **18**, 4405–4414.
- Mering, J. (1949) L'interférence des rayons X dans les systèmes à stratification désordonnée. *Acta Crystallographica*, **2**, 371–377.
- Mostarih, R. and de Roy, A. (2006) Thermal behavior of a zinc-chromium-sulfate lamellar double hydroxide revisited as a function of vacuum and moisture parameter. *Journal of Physics and Chemistry of Solids*, **67**, 1058–1062.
- Oswald, H.R. and Asper, R. (1977) *Preparation and Crystal Growth of Materials with Layered Structures* (R.M.A. Leith, editor). Riedel Publishing Company, Dordrecht, The Netherlands, pp. 71–140.
- Radha, S. and Kamath, P.V. (2013) Polytypism in sulfate-intercalated layered double hydroxides of Zn and M(III) (M = Al, Cr): Observation of cation ordering in the metal hydroxide layers. *Inorganic Chemistry*, **52**, 4834–4841.
- Radha, S., Milius, W., Breu, J., and Kamath, P.V. (2013) Synthesis and reversible hydration behavior of the thiosulfate intercalated layered double hydroxide of Zn and Al. *Journal of Solid State Chemistry*, **204**, 362–366.
- Reichle, W.T. (1986) Synthesis of anionic clay minerals (mixed metal hydroxides, hydrotalcite). *Solid State Ionics*,

- 22, 135–141.
- Roussel, H., Briois, V., Elkaim, E., de Roy, A., and Besse, J.P. (2000) Cationic order and structure of [Zn-Cr-Cl] and [Cu-Cr-Cl] layered double hydroxides: An XRD and EXAFS study. *Journal of Physical Chemistry B*, **104**, 5915–5923.
- Roussel, H., Briois, V., Elkaim, E., de Roy, A., Besse, J.P., and Jolivet, J.P. (2001) Study of the formation of the layered double hydroxide [Zn-Cr-Cl]. *Chemistry of Materials*, **13**, 329–337.
- Serna, C.J., Rendon, J.L., and Iglesias, J.E. (1982) Crystal-chemical study of layered $[Al_2Li(OH)_6]^+X^- \cdot nH_2O$. *Clays and Clay Minerals*, **30**, 180–184.
- Sideris, P.J., Nielson, U.G., Gan, Z., and Grey, C.P. (2008) Mg/Al ordering in layered double hydroxides revealed by multinuclear NMR spectroscopy. *Science*, **321**, 113–117.
- Sideris, P.J., Blanc, F., Gan, Z., and Grey, C.P. (2012) Identification of cation clustering in Mg-Al layered double hydroxides using multinuclear solid state nuclear magnetic resonance spectroscopy. *Chemistry of Materials*, **24**, 2449–2461.
- Treacy, M.M.J., Newsam, J.M., and Deem, M.W. (1991) A general recursion method for calculating diffracted intensities from crystals containing planar faults. *Proceedings of the Royal Society, London*, **A433**, 499–520.
- Treacy, M.M.J., Deem, M.W., and Newsam, J.M. (2000) *Computer Code DIFFAX, Version 1.807*. NEC Research Institute, Inc., Princeton, New Jersey, USA.
- Vucelic, M., Jones, W., and Moggridge, G.D. (1997) Cation ordering in synthetic layered double hydroxides. *Clays and Clay Minerals*, **45**, 803–813.
- Weiss, A. (1963) A secret of Chinese porcelain manufacture. *Angewandte Chemie*, **75**, 755–762.

(Received 13 September 2013; revised 25 February 2014; Ms. 812; AE: M. Plötze)